UNIVERSITY OF CALIFORNIA, SAN DIEGO

Group-Level Analysis of Source-Resolved Event Related Potential and Brain Connectivity

A Thesis submitted in partial satisfaction of the requirements

for the degree Master of Science

in

Bioengineering

by

Clement Lee

Committee in charge:

Gert Cauwenberghs, Chair
Todd Prentice Coleman
Tzyy-Ping Jung
Scott Makeig

2016

The Thesis of Clement Lee is approved, and it is acceptable in quality and form for publication on microfilm and electronically:

_____

_____

_____

_____

Chair

University of California, San Diego

2016

DEDICATION

To my mother and late father, whose sacrifices afforded me this possibility.

TABLE OF CONTENTS

LIST OF FIGURES

LIST OF TABLES

ACKNOWLEDGEMENTS

I would like to thank my thesis committee members for their time and feedback. In particular, I am grateful to my departmental advisor and committee chair, Professor Gert Cauwenberghs, who always took the time to advise me whether in person or by e-mail. I would also like to express my gratitude to Dr. Scott Makeig for his invaluable mentorship, and specifically his sincere advice to stay grounded throughout the creative process of scientific exploration. In addition, while Professor Ratneshwar Lal is not on my committee, I have to thank him for advising me, as an undergraduate, to get in touch with the Swartz Center for Computational Neuroscience when he noticed my interest in Neuroscience, and for supporting part of my graduate studies by awarding me a Teaching Assistantship for his Biomedical Optics and Imaging course.

This work would not have come to fruition without the many members of the Swartz Center for Computational Neuroscience and the Institute for Neural Computation. First and foremost I would like to thank Dr. Makoto Miyakoshi for appreciating my enthusiasm when my abilities were wanting as an undergraduate, for allowing me to partake in many of his ongoing projects, and for guiding me through the research process. Next I have to thank Shawn Hsu, Masaki Nakanishi, Cory Stevenson, and Luca Pion-Tonachini, for the time spent at and in preparation for Milan's 2015 IEEE Engineering in Medicine and Biological Society Conference. I have to thank Professor Cauwenberghs and Dr. Makeig again here, for their financial support of my conference attendance. Of course, I cannot leave out Ozgur Balkan (whom I may as well call iOzgur

since he now works for Apple), Ramon Cancino-Martinez, Professor Hirokazu Tanaka, and Johanna Wagner, who shared an office with me at the lab and always answered my questions, regardless of how nonsensical the questions may have been. I also have to thank everyone who has hosted or attended the lab's tea time and contributed to the refreshments not only for the body but also for the mind. Last but not least, I would like to thank my dear friends Matthew Choi and Sarah Hsu, who have proofread many of my written pieces and shaped my identity as a writer since I immigrated to America a little over a decade ago.

Chapter 2, in part, is a reprint of the material as it appears in C. Lee, M Miyakoshi, A. Delorme, G. Cauwenberghs and S. Makeig. "Non-parametric group-level statistics for source-resolved ERP analysis," in 37th Annual International Conference of the IEEE Engineering in Medicine and Biology Society., Milan., 2015, pp. 7450-7453. The thesis author was the primary investigator and author of this paper.

The work in Chapter 3 was carried out under the guidance of Makoto Miyakoshi, Gert Cauwenberghs, and Scott Makeig. The Source Information Flow Toolbox (SIFT) and Measure Projection Toolbox (MPT) were created by Tim Mullen and Nima Bigdely-Shamlo, respectively; the thesis author would like to thank Tim Mullen and Nima Bigdely-Shamlo for their advice, via e-mail and in-person at Qusp. The thesis author was the primary investigator and author of this work.

ABSTRACT OF THE THESIS

Group-Level Analysis of Source-Resolved

Event Related Potential and Brain Connectivity

by

Clement Lee

Master of Science in Bioengineering

University of California, San Diego, 2016

Professor Gert Cauwenberghs, Chair

Electroencephalography (EEG) has made much progress since the 1920s, when Dr. Hans Berger began his exploration of what he initially thought of as supernatural psychic energy. Now almost a century later, most laypeople are familiar with the concept of EEG; some may even casually say “we’re on the same wavelength” when in agreement with each other. In the scientific community, rigorous data analysis has protected EEG from dismissal as a pseudoscience. Furthermore, the successful

application of independent component analysis (ICA) to EEG data and the subsequent release of EEGLAB, a GUI-based Matlab toolbox for processing EEG data, allows for and facilitates source-level analysis. Today, the lowering costs of data acquisition and storage continue to drive demand for tools and methods to process large datasets. Researchers may default to channel-level analysis, but some types of analysis (e.g. brain connectivity) are more sensible at the source-level. Each chapter in this thesis documents a method of analysis for an EEGLAB STUDY (a grouping of EEG datasets, source-resolved by ICA, for comparative analysis). Chapter 2 shows the EEGLAB plug-in *std_envotpo*, which creates STUDY-level envelope plots of the topography, and its sub-function *statPvaf*, which allows for non-parametric statistical analysis of the percent variance accounted for. Chapter 3 explores parameter selection in a new data processing pipeline, which utilizes the Source Information Flow Toolbox (SIFT) and Measure Projection Toolbox (MPT) to calculate brain connectivity estimators at the group level.

Chapter 1

Introduction

Electroencephalography (EEG) recording is high in temporal resolution and typically less costly compared to other brain imaging techniques such as positron emission tomography (PET) or functional magnetic resonance imaging (fMRI), but is limited in spatial resolution because recordings are taken from electrodes placed on the scalp. Furthermore, recorded signals are significantly affected by volume conduction in the brain and scalp mixing. In 1996, Makeig et al. pioneered the application of Independent Component Analysis (ICA) to scalp recorded EEG data [1]. With its ability to identify and separate not only brain sources but also artifactual independent components (ICs), ICA trivializes EEG's limitations in volume conduction and scalp mixing and became a powerful tool in EEG analysis. In 2004, Delorme and Makeig published EEGLAB, a freely available toolbox and graphic user interface running on Matlab (The MathWorks Inc., Natick, MA) with a focus on open source development of signal processing tools for ICA-driven EEG research [2]. Since then, EEGLAB has been downloaded in at least 88 countries and cited over 5,500 times. The toolbox continues to grow, with many users suggesting or submitting plug-ins to revise or add new functions to EEGLAB.

Although ICA continues to gain popularity, some EEG researchers still prefer channel-based analysis. One possible reason is that ICA-based approach complicates the subsequent group-level analysis because of inconsistent number and location of brain-ICs (i.e. effective source EEG activities) across subjects; addressing these issues requires new data processing methods. Some users may feel that EEGLAB's solution for comparing data collected from multiple subjects is too complicated or cumbersome: ICs from different subjects must be clustered based on selected parameters, unlike channel-level activity which can be reconciled between subjects simply by knowing the channel locations. To address the aforementioned concerns, the EEGLAB STUDY (a grouping of comparable EEG data sets for use in comparative analysis between groups, conditions, and sessions) is continually updated with new tools to further facilitate group-level analysis [3]. Each chapter in this thesis documents a method of analysis supported by the EEGLAB STUDY.

In Chapter 2, we demonstrate the EEGLAB plug-in *std_envtopo,* a tool for creating STUDY-level envelope plots of the topography, where maximum and minimum channel values and projected values from IC clusters are plot against event related potential (ERP) latencies. We explore *std_envtopo*'s new sub-function *statPvaf*, which is used to test for significant differences in main effect subtraction or interactions using non-parametric bootstrap statistics on percent variance accounted for (*pvaf*, a measure used to rank IC cluster contributions).

In Chapter 3, we explore an EEG preprocessing pipeline for analyzing brain connectivity. We use the Source Information Flow Toolbox (SIFT) to compute brain connectivity estimators and use Network Projection, an extension of the Measure Projection Toolbox (MPT), to reconcile the measures amongst subjects at the group-level. Throughout this multi-step process, selecting different parameters can yield vastly different results. We test the effects of parameter selection using simulated data, and demonstrate the use of the pipeline with actual data from a visual hemifield presentation task.

While much focus is on improving algorithms and applying real-time data processing for use in wearables and brain machine interfaces, continued improvement of batch processing techniques remains significant in encouraging and facilitating source-level analysis.

Chapter 2

Non-Parametric Group-Level Statistics for Source-resolved ERP Analysis

2.1 Abstract

We have developed a new statistical framework for group-level event-related potential (ERP) analysis in EEGLAB. The framework calculates the variance of scalp channel signals accounted for by the activity of homogeneous clusters of sources found by independent component analysis (ICA). When ICA data decomposition is performed on each subject's data separately, functionally equivalent independent components (ICs) can be grouped into EEGLAB clusters. Here, we report a new addition (*statPvaf*) to the EEGLAB plug-in *std_envtopo* to enable inferential statistics on main effects and interactions in event related potentials (ERPs) of IC processes at the group level. We demonstrate the use of the updated plug-in on simulated and actual EEG data.

2.2 **Introduction**

Independent component analysis (ICA) has been used in EEG analysis since 1996 [1]. ICA can be understood as a process of maximizing non-Gaussianity. The motivation for its application to EEG data is as follows: scalp-recorded EEG signals sums volume-conducted projections of effective brain sources, each typically indexing synchronous electrical activity across a cm-scale cortical patch, and of non-brain sources (from scalp muscles, heart, eye movements and eye blinks, sweating, as well as external non-physiological noise sources). The recorded data signals are linear mixtures of these independent activities. By the central limit theorem, such a mixture approaches a Gaussian distribution. However, typically Gaussian distributions arise only from mixing, while the brain source signals of interest are non-Gaussian [4], [5]. Empirical evidence has shown that mutual information reduction by ICA is associated with returning components with near-dipolar scalp maps [6].

Using ICA results, we can ask what contribution is made to the scalp EEG signals by selected brain independent components (ICs) and by clusters of similar ICs found in some or all subjects. The function *std_envtopo* in EEGLAB quantifies the source contribution to the scalp signals in terms of percent variance accounted for (pvaf). For a given IC cluster,

$$pvaf = 100 - 100 * V_{remainingClusters}/V_{allClusters}. \quad (2.1)$$

Here, $V_{remainingClusters}$ is the mean of variances across summed projections of all other clusters, and $V_{allClusters}$ is the mean of variances across the summed projections of all clusters.

However, there has been no statistical framework to test the significance of the pvaf measure or its group/condition differences and interactions. Part of the reason is the sub-additivity of signal variance, var(A+B) < var(A) + var(B). We have therefore developed a new statistical framework for measuring and comparing the pvaf's of IC clusters in an EEG STUDY (in EEGLAB, a grouping of comparable EEG data sets for use in comparative analysis). The purpose of the framework is to compute the statistics of differences in source IC contributions to the scalp data at the group level. We apply it here to event-related potential (ERP) averages of short data epochs time-locked to some class of experimental events of interest.

2.3 **Methods**

A. Data Processing in EEGLAB: std_envtopo and statPvaf

1) *IC clustering in an EEGLAB STUDY*: Fig. 2.1 shows the major processes involved in obtaining pvaf statistics. After EEG data collected from a group of subjects are preprocessed, ICA decomposition is performed on each subject's data to separate brain and non-brain source activities linearly mixed at scalp sensors. Identified ICs have maximally independent activity time series and fixed scalp topographies or

maps [1]. Next, each independent component scalp map is fit to the scalp projection of an equivalent current dipole using DIPFIT 2.3 (an EEGLAB plug-in using Fieldtrip toolbox functions) [6]. IC clusters can then be created for the EEGLAB STUDY by grouping similar ICs based on similarities in equivalent dipole locations, scalp maps, mean log power spectra, event related potentials (ERPs), etc. [3].

2) *Envelope and topography plotting: std_envtopo*: The main purpose of the *std_envtopo* function is to plot the envelopes of the summed scalp projections of selected IC clusters overlaid by the envelopes of scalp projection and the summed scalp maps of the largest-contributing IC clusters. Scalp recorded data (X) are modeled by

$$X = W^{-1}S, \tag{2.2}$$

where W^{-1} is the inverse of the ICA unmixing matrix and S is the matrix of source activities. If the number of ICA components is less than number of data channels, $W^{-1}$is the pseudo-inverse weight matrix. At the STUDY level, scalp projections are calculated by convolving W^{-1} with non-artifactual component S. Because subjects may have had differing numbers of channels entered into the analysis, comparable scalp topographies for each IC are generated by interpolating the individual subject scalp map channel positions using Matlab (The MathWorks Inc., Natick, MA) function *griddata*. Fig. 2.2 shows the user interface of the *std_envtopo* plug-in as called from EEGLAB. The default option is to generate output for each STUDY variable combination (Fig. 2.3ii), but a main or interaction effect difference can be computed instead (Fig. 2.3iii). In the graphical output (Fig. 2.3i, 2.3ii, 2.4iii), black outer traces show the maximum and minimum channel values at each ERP latency, and coloured traces show the maximal

and minimal projected channel values for the most strongly-contributing IC clusters; straight lines match cluster envelopes to their respective cluster scalp maps, labels, and sorting variable values; dashed vertical lines indicate the latency range in which the cluster projections are ranked.

3) Bootstrap statistics in statPvaf: When a main effect subtraction or an interaction is specified in *std_envtopo*, the *statPvaf* sub-function can be run to perform inferential statistics on pvaf. We explain *statPvaf* by examining an effect of between-group conditions, namely Group1 Condition1 – Group2 Condition1 for a STUDY with a 2X2 design. First, an IC stack is created by combining ICs depending on the STUDY variable of interest; for our between-group difference, the common variable is Condition. In each of the 5,000 iterations of bootstrapping for each cluster of interest, a surrogate IC set is generated by random combination of ICs from the IC stack. The surrogate IC set is then used to calculate surrogate projections. Fig. 2.3iv shows a schematic for surrogate generation: in our example case, the golden boxes represent ICs from Group1 while the light blue boxes represent those from Group2. In the original data, the difference is between 3 Group1 ICs and 2 Group2 ICs; in the surrogate data, the Group variable is ignored and the difference is between any 3 Condition1 ICs and any other 2 Condition1 ICs. By randomly selecting ICs in this way, we can test the null hypothesis of statistical insignificance in Group differences.

B. Simulated STUDY with 2 x 2 Design

A simulated EEGLAB STUDY was created to test *std_envtopo*. The STUDY features a 2 x 2 design with 20 subjects, each with 20 ICs. The subjects were divided between Group1 and Group2 (ten subjects per group), and each subject's ICs were divided between Condition1 and Condition2 (ten ICs per condition). The 400 total ICs were separated into 5 clusters (80 ICs per cluster), and all clusters were assigned the same scalp topography to prevent differences in projection. As shown in Fig. 2.3i, Clusters 1, 2, 4, and 5 are composed of identical ICs in all four group-condition combinations, but Cluster 3 is composed of differing ICs.

To confirm the structure of the STUDY design, we first used *std_envtopo* to create plots for each group-condition combination. Then, with the same latency window, we plotted the largest contributing cluster in the interaction of condition x group, namely (Group2 Condition2 – Group2 Condition1) – (Group1 Condition2 – Group1 Condition1).

In this simulation, it is predicted by definition that the pvaf of Cluster 3 in the difference ERP will always be 100% because the contribution of all other clusters are simulated to be exactly zero after subtraction, regardless of how the how the ICs are shuffled and projections are subtracted. The parameters are shown in Table 2.1.

C. Application to Actual STUDY with 2 x 2 Design

The duration mismatch negativity task was performed on 42 non-psychiatric subjects (NCS) and 47 schizophrenia patients (SZ) [7]. The factorial design of the

experiment was 2 x 2 mixed design; stimulus types (Standard, Deviant) as a within-subject condition vs. group as a between-subject condition. *std_envtopo* and *statPvaf* were applied to examine the interaction of stimulus types x group, namely (Deviant Patient – Standard Patient) – (Deviant Control – Standard Control). The parameters are shown in Table 2.1.

2.4 **Results**

Fig. 2.3 shows the *std_envtopo* results for the simulated study. The envelope plots for all Group-Condition combinations in Fig. 2.3ii show the latencies at which each cluster has maximum contribution. We omitted the scalp maps since they were simulated to be consistent across all clusters. As expected, Cluster 3 accounted for 100% of the variance in the interaction of condition x group (Fig. 2.3iii). Δ-pvaf is 0%. In the envelope plots for all group-condition combinations, Clusters 1 through 5 showed maximal contribution during their respective half cycle, and both the inner and outer envelopes in the 3rd half cycle reflect the influence of Cluster 3's unique ERP design. In the envelope plot of the interaction, there is no signal except for the latency corresponding to the 3rd half cycle of the sine wave. Since this latency window corresponds to Cluster 3, the plot and the calculated pvaf value match the expectation that only Cluster 3 would have a nonzero interaction term and account for all of the variance in the interaction.

For the interaction of the actual data, peak in Deviant (D) condition in Control group is the largest, followed by Deviant in Patient group, and finally by Standard (S)

condition in both Control and Patient groups. The interaction term contribution of the Mid-Cingulate cluster was the largest with a pvaf of 32%. Fig. 2.4i shows the skewed pvaf(A-B) distribution; we attribute this to the Cauchy-Schwarz inequality. The histogram in Fig. 2.4ii shows the distribution of surrogate Δ-pvaf values, ranging from -18% to 36%. In line with the central limit theorem, the surrogate Δ-pvaf distribution approaches a Gaussian form. The upper and lower bounds of the confidence interval were 23% and -2% respectively. In the original data, pvaf was 10% and 22% in Patient and Control group respectively, giving a Δ-pvaf of -12%. This difference reached statistical significance at $p<0.001$ (Fig. 2.4iii).

2.5 **Discussion**

We demonstrated how *std_envtopo* and stdPvaf work using simulated and actual data. We also compared the two approaches to construct surrogate data, namely pvaf(A - B) and pvaf(A) - pvaf(B) (i.e. Δ-pvaf), and showed that Δ-pvaf is preferable since it does nto suffer from the Cauchy-Schwarz inequality and has a Gaussian distribution. It should also be noted that this is the first dedicated explanation of the *std_envtopo* function used in EEGLAB. Its significance is to bridge the 'projected' scalp channel measures to the underlying source-resolved brain EEG activities by computing the accounted variance of the latter in the former. The methods presented address a previously unmet need to perform inferential statistics on pvaf, a measure useful for determining which IC clusters to analyze. The addition of *statPvaf* to *std_envtopo* may further encourage and facilitate the use of ICA for EEG analysis. In future, statistical

methods of multiple comparison correction such as the Bonferroni-Holm method will be incorporated to refine multi-cluster *statPvaf*. The user interface of *std_envtopo* will also be improved to allow more intuitive option selection.

2.6 **Conclusion**

Functions *std_envtopo* and *statPvaf* enable us to ask how much ERP variance is accounted for by source-resolved EEG activities, to identify largest-contributing IC clusters, and to determine whether their contributions are significantly different across conditions. They connect effective EEG sources to their scalp projections by showing the contribution of the former to the latter.

2.7 **Acknowledgments**

The authors would like to thank Dr. Gregory Light and Dr. Anthony Rissling for permission to use their data here. Chapter 2, in part, is a reprint of the material as it appears in C. Lee, M Miyakoshi, A. Delorme, G. Cauwenberghs and S. Makeig. “Non-parametric group-level statistics for source-resolved ERP analysis,” in 37th Annual International Conference of the IEEE Engineering in Medicine and Biology Society., Milan., 2015, pp. 7450-7453. The thesis author was the primary investigator and author of this paper.

2.8 **Figures**

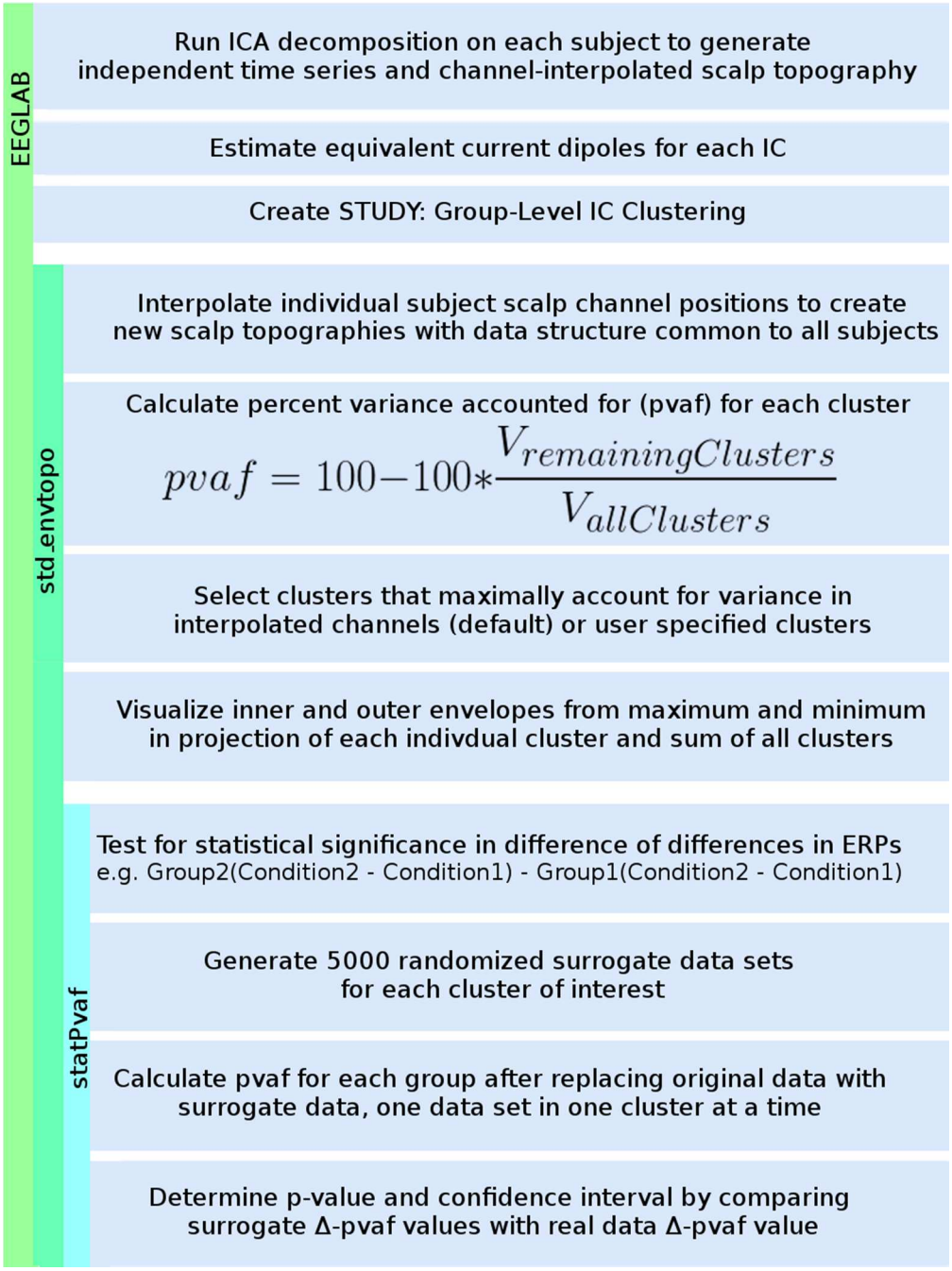

Figure 2.1. Pipeline of major processes in toolbox EEGLAB, plug-in std_envtopo, and sub-function statPvaf.

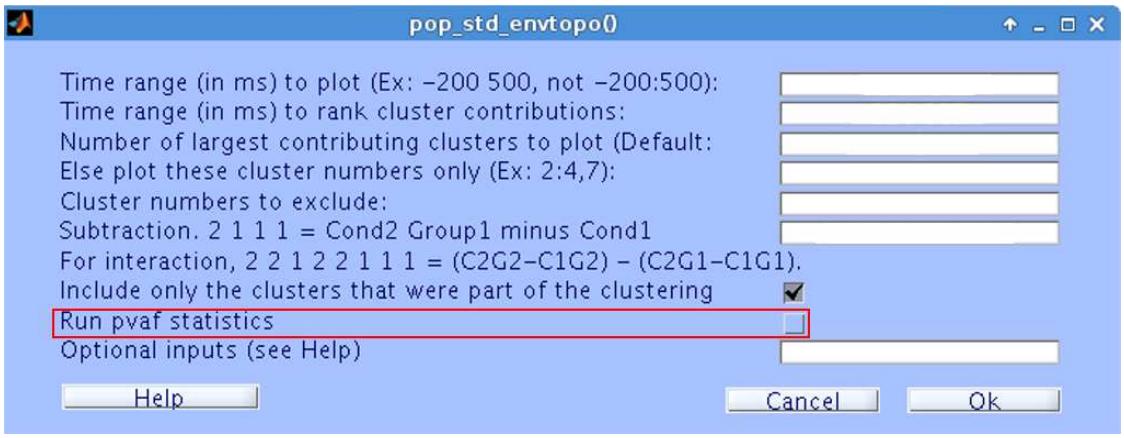

Figure 2.2. std_envtopo user interface. The default option for statPvaf is off.

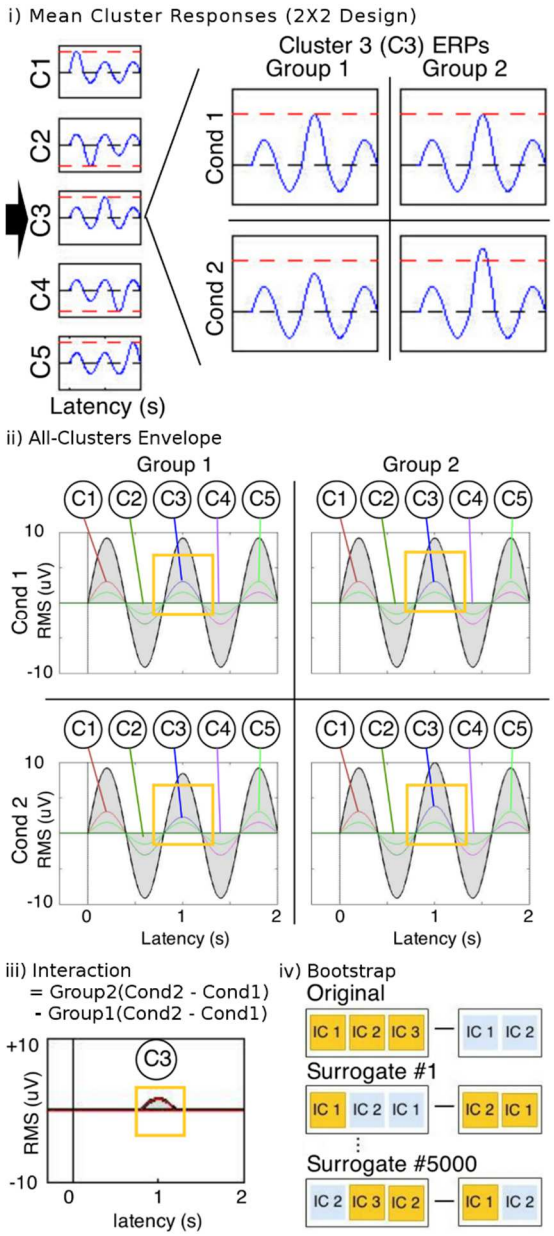

Figure 2.3. STUDY design and std_envtopo for simulated data. i) Mean cluster responses. The mean response of each cluster is a 1.25Hz sine wave with amplitude of 1, except for a specified half cycle where the amplitude is doubled. Clusters 1, 2, 4, and 5 are composed of identical ERPs in all four group-condition combinations, but Cluster 3 is composed of differing ERPs: for Condition2, the maximum amplitude is smaller in Group1 and larger in Group2. ii) Envelope plots for all Group-Condition combinations. The golden boxes highlight the latencies for which Cluster 3 is different. iii) Interaction envelope plot showing the difference of differences. The golden box highlights the expected contribution from Cluster 3. iv) Schematic of surrogate data generation in bootstrapping. Difference in background colours represent a difference in one STUDY variable. Note that ICs are chosen with replacement by definition of bootstrapping.

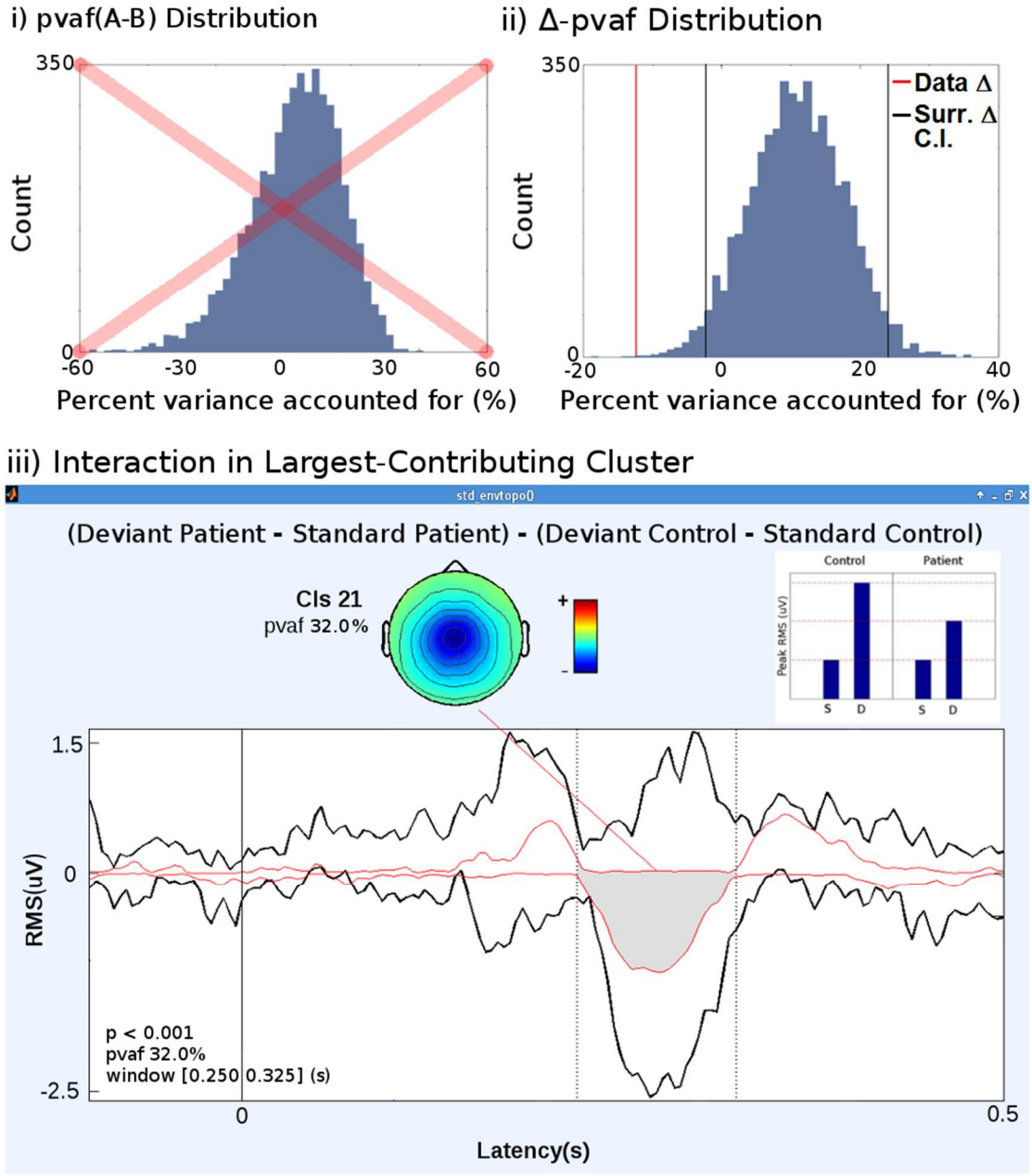

Figure 2.4. std_envtopo and statPvaf for real data. i) Skewed distribution in pvaf(A-B). ii) Histogram of surrogate Δ-pvaf distribution. The black lines indicate the confidence interval and the red line marks the data Δ-pvaf (-12.4%). iii) std_envtopo plug-in result. Between 0.250 and 0.325s, the interaction in the Midcingulate cluster is statistically significant and accounts for 32.0% of the variance in scalp projection differences.

2.9 **Tables**

Table 2.1. std_envtopo parameters

Parameters	**Data Set**	
	Simulation	*Actual*
Time range (in ms) to plot:	[-300 2000]	[-200 500]
Time range (in ms) to rank cluster contributions:	[0 2000]	[220 325]
Number of largest-contributing clusters to plot	5	1
Factorial Design	2 x 2 Interaction	2 x 2 Interaction
Number of clusters used in *statPvaf*	1	1

Chapter 3

Group-Level Graph Theoretical Brain Connectivity Analysis

3.1 Abstract

We explore a recently developed data analysis framework for graph theoretical connectivity analysis of group-level source-resolved EEG. The framework leverages pre-existing EEGLAB toolboxes to compute and visualize connectivity estimators. Source Information Flow Toolbox (SIFT) fits multivariate autoregressive (MVAR) models and calculates connectivity estimators; and Network Projection, an extension of the Measure Projection Toolbox (MPT), obviates issues associated with comparing independent components (ICs) from different datasets. In this chapter, we compare two common connectivity measures, the direct directed transfer function (dDTF08) and the renormalized partial directed coherence (RPDC); examine the full width at half maximum parameter for Network Projection using simulated data; and apply the pipeline to actual data from a visual hemifield presentation task.

3.2 Introduction

Despite the growing interest in brain connectivity analysis, the multitude of brain connectivity estimators and data processing methods complicates the development of a standard. Furthermore, group-level analysis is complicated by the inconsistent number and location of brain-ICs (i.e. effective source EEG activities) across subjects. The Source Information Flow Toolbox (SIFT) [3] in EEGLAB contains a suite of functions and accompanying graphical user interface (GUI) to preprocess data, fit multivariate autoregressive (MVAR) models, estimate connectivity measures, compute statistical significance, and visualize results [3]. We build upon SIFTs functionality and examine, at the group level, the estimators direct directed transfer function (dDTF08) [8] and renormalized partial directed coherence (RPDC) [9], which are modified versions of directed transfer function (DTF) [10] and partial directed coherence (PDC) [11], respectively.

Classically, EEG scalp recordings can be compared between multiple sessions or multiple subjects based on the standardized channel locations defined by international 10-20 system and its extensions [12], [13]. This practice holds true for connectivity estimators since DTF - and by extension other frequency based connectivity estimators - has been shown to be unaffected by volume conduction [14]. However, an Independent Component Analysis (ICA) based approach would result in effective source connectivity whereas a channel-based approached would result in connectivity of signals affected by volume conductance and scalp mixing. When analyzing at the source

level, extra effort is needed to reconcile independent components (ICs) between subjects and or sessions; unlike standardized channel locations, ICs and their equivalent dipole locations can be inconsistent among datasets. EEGLAB offers support for multi-subject or multi-session data with implementations such as the STUDY structure and IC clustering.

One proposed way of achieving spatial consistency of EEG dynamics is by using Network Projection [15], an extension of the Measure Projection Toolbox (MPT) which can operate on anatomical regions of interests, akin to functional magnetic resonance images (fMRI) voxel by voxel analysis. Instead of a single point, each dipole is modeled by a Gaussian density, defined by its full width at half maximum (FWHM) following conventions in the field of neuroimaging, on a substrate of 76 anatomical regions of interest generated based on the Automated Anatomical Labeling (AAL) atlas. When modeling an IC as a density, a critical point is choosing the appropriate FWHM. If too small, the IC may as well be modeled as a dipole; if too large, spurious results may arise. For example, Fig. 3.1 shows the dDTF08 connectivity results of a simulated dataset processed with an unsuitably large FWHM of 16mm. In this dataset, the Frontal Mid Orbital Left drives Occipital Superior Left from 0 to 0.75s and Paracentral Lobule Left from 0.75 to 1.25s. Frontal Mid Orbital Left was not modeled to drive Precuneus Left, but the pair appears to be connected and displays the union of connectivity measures from the neighboring regions. Because of an inappropriate FWHM, the spurious connection lasts longer compared to each of the actual connections. We simulate data to further study the effects of selecting different FWHM.

3.3 **Methods**

A. Brain Connectivity Estimators

The two brain connectivity estimators examined, dDTF08 [8] and RPDC [9], are both multivariate methods based on Granger causality. A MVAR model is fitted to the EEG signal before the estimators can be calculated. A process with *k* number of ICs are represented as a vector *X(t)* where

$$X(t) = [X_1(t), X_2(t), \dots, X_k(t)]^T. \tag{3.1}$$

The MVAR model can then be expressed as

$$X(t) = \sum_{i=1}^{p} A(i)X(t-i) + E(t), \tag{3.2}$$

where *p* is the model order, *A(i)* are the model coefficients, and *E(t)* is a vector of white noise processes. We set *A(0) = I* to obtain

$$\sum_{i=0}^{p} A(i)X(t-i) = E(t) \tag{3.3}$$

and transform (3.4) to the frequency domain to obtain

$$X(f) = A^{-1}(f)E(f) = H(f)E(f), \tag{3.4}$$

where

$$A(f) = \sum_{i=0}^{p} A(i) \exp(-j2\pi f \Delta t i) \,, \tag{3.5}$$

and *H* is the transfer matrix of the system. The DTF family operate on H_{ij}, whereas the PDC family operate on A_{ij}; the indices point to the causality from source *j* to sink *i*. dDTF08 is DTF renormalized and multiplied by partial coherence to correct for cascade flow in DTF, which does not distinguish between direct and indirect causation. RPDC is PDC renormalized to represent measures with respect to all inflows to the sink *i* instead of outflows from source *j*. SIFT [3] was used to fit the MVAR model for each subject and to calculate the respective connectivity estimates; segmentation-based adaptive MVAR modelling was used to model locally stationary data.

Next we propagated connectivity measures to the group level and perform statistical analysis. We used Network Projection [15] to model the ICs as Gaussian densities on a grid of 76 x 76 anatomical regions, or in graph theoretical terms, edges. We selected edges that contained a threshold dipole pair density value in a percentage of subjects. One method of statistical analysis is to test the convergence quantity calculated by Network Projection; convergence is calculated using dipole pair probability density and measure similarity (i.e. time-frequency correlations in connectivity estimate), and is higher for areas homogenous across subjects. One weakness in this method was that time-frequency points were collapsed into one convergence value for each edge, resulting in varying statistical significance when different latency or frequency ranges were selected. The convergence test could also be

criticized for violating sound practice of statistics by performing circular analysis, or double dipping. Thus, a second method which tests each time-frequency point was chosen. For a bootstrap test, group baseline data were created by concatenating all subjects' mean-subtracted baseline time-frequency connectivity estimates in a following way: group baseline data = frequency x (baselineDatapoints x subjects). For a single condition, baseline-corrected connectivity estimates from all subjects were tested against the group baseline data. For two conditions, in addition to the single condition tests, baseline-corrected connectivity estimates from one condition was tested against estimates from the other. We visualized results by plotting t-scores obtained from the bootstrap test [16]; from here, we refer to plots produced by this method as time-frequency t-score plots. An adaptation of the generalized familywise error rate [17] was used for multiple subject comparison: a selected number of false positives (u) were allowed, but we set a cluster size threshold which dictated how many significant time-frequency points must exist in a neighborhood for an edge to be considered significant.

B. Simulated Data

We simulated datasets containing 4-dimensional VAR[2] processes using SIFT's built in simulation function. Each set contained 20 subjects; each subject had nine ICs and 100 trials sampled at 100Hz from -1 to 2s. IC1 caused IC3 at 10 Hz and IC2 caused IC4 at 25 Hz; the ICs were modeled as damped oscillators from 0 to 2s using the equations:

$$x_1(t) = 2 * \exp(-0.1\cos(0.2\pi)) * x_1(t-1) - \exp\big(-0.2x_1(t-2)\big) + e_1(t)$$

$$x_2(t) = 2 * \exp(-0.1\cos(0.5\pi)) * x_2(t-1) - \exp\big(-0.2x_2(t-2)\big) + e_2(t)$$

$$x_3(t) = 2 * \exp(-0.5\cos(0.2\pi)) * x_3(t-1) - \exp\big(-x_3(t-2)\big) + (0.3 * \sin(0.02\pi t + 0.3) * x_1(t-2) + e_3(t)$$

$$x_4(t) = 2 * \exp(-0.5\cos(0.5\pi)) * x_4(t-1) - \exp\big(-x_4(t-2)\big) + (0.3 * \sin(0.02\pi t + 0.3) * x_2(t-2) + e_4(t), \quad (3.6)$$

where e(t) is a vector of Gaussian noise processes. The baseline period of -1 to 0s in IC1 through IC4 was populated by pink noise, which is typically observed in brain ICs. IC5 through IC9 were simulated as noise for the whole epoch.

We processed the simulated datasets in multiple ways to study the interaction between Gaussian density FWHM and maximum dipole location error. Equivalent dipoles were located near selected anatomical region centroids in the left hemisphere. IC1 through IC4 were placed near the Frontal Mid Orbital, Frontal Inferior Triangularis, Cuneus, and Angular Gyrus, respectively. To simulate dipole location estimation errors, the signal-containing dipoles were uniformly distributed around the centroids in a sphere. 3 test cases were generated with sphere radii 0, 10, and 30mm. 0mm was chosen as the best case scenario, 10mm was chosen based on scale of the median dipole source location errors reported in [18], and 30mm was chosen to portray an extreme example of poor dipole fitting or IC-inconsistency between subjects (Nima Bigdely-Shamlo, personal communication, Qusp, July 2016). When fitting dipoles in EEGLAB, it is possible to limit dipole fitting to within the brain; this option was not used in the simulation because a uniform distribution was desired.

The data were fed into the pipeline: both dDTF08 and RPDC were calculated using SIFT with a 1s window length, 0.02s step size, and a frequency range of 2 to 50 Hz in 30 log-scaled bins. Each of the 3 maximum dipole location error cases was modeled with 3 Gaussian FWHM, 8, 16, and 24mm, for a total of 3 x 3 cases; 8mm is the length of a single voxel in the grid used by Network Projection. In each case, at least 90% of dipole pair densities were represented in the final results. Statistics was not used to threshold the final results.

C. Actual Visual Hemifield Data

We used 22 of the 24 collected datasets from the visual hemifield study [19]. The study featured two levels of Domain (Face and Cup), three levels of Familiarity (Self, Familiar, and Unfamiliar), and three levels of Visual Field (Left, Right, and Bilateral). We applied the pipeline to examine the significant differences in effective brain connectivity between Visual Field conditions Bilateral and Left, Bilateral and Right, and the Left and Right. The three levels of Familiarity and the two levels of Domain were collapsed.

Since Barnett and Seth [20] showed that filtering EEG data results in undesired complications in connectivity analysis, EEG data were preprocessed using an adaptation of the early-stage EEG processing pipeline (PREP) [21]. After the data were imported into EEGLAB, we used high pass filtering and the *cleanline* plug-in to generate a noise template of the line noise, cathode ray tube monitor artifacts, and their harmonics, with frequencies of 60, 100, 120, 180, 200, and 240Hz; we avoid low-pass filtering by

subtracting this noise template from the original unfiltered data. To clean drift noise while avoiding high-pass filtering, we used linear detrending with a segment size of 0.5s and step size of 0.125s. Next, spike artifacts were removed by temporal interpolation with the *ARfitStudio* plugin. The data were then resampled from 500 to 100Hz, and Artifact Subspace Reconstruction was used to remove non-stationary high-variance signals with a threshold of five standard deviation. We perform ICA decomposition, and the data from the 22 subjects were epoched and divided into three datasets based on the Visual Field conditions of Bilateral, Left, or Right.

dDTF08 was calculated using window length of 1s, step size of 0.02s, and frequency range of 2 to 50 Hz in 30 log-scaled bins. The dipoles were modeled with Gaussian FWHM of 8mm, and edges containing 0.0005 dipole pair density in 50% of subjects were selected. GFWER was used for multiple comparison correction: 10 false positives were allowed, and the cluster size threshold size 10 time-frequency points.

3.4 **Results**

A. Simulated Data

Fig. 3.2 shows the dDTF08 and RPDC time-frequency t-score plots for a single subject. While both methods captured the modeled 1Hz modulation in the time domain, dDTF08 is much more specific and accurate in the frequency domain. RPDC seemed to blur towards the lower frequency range, and also showed a distortion above 40Hz; these frequency distortions are reproducible in multiple actual datasets, including data from the visual hemifield presentation task (not shown). The reasons for RPDC's failures are

unknown (Tim Mullen, personal communication, Qusp, July 2016), and issues persisted even when different MVAR modeling parameters were selected. Clearly, dDTF08 is the superior connectivity estimate for our applications.

Although we modeled the 9 ICs around region centroids within the left hemisphere, modeling the ICs as densities with dipole location errors resulted in inter and intra hemispheric connectivity. Table 3.1 shows the total number of hemispheric interactions and categorizes them based on direction: left to left, left to right, right to left, and right to right. Except for the 30mm maximum dipole location error case, the number of total edges increases with higher FWHM. Fig. 3.3 shows the 3 x 3 cases of data processed to study the interaction between FWHM and maximum dipole location error. Each plot contains 10 x 10 edges representing connectivity near the ICs. The colour of each point represents the t-score from the bootstrap testing, and colour scales are consistent across each dipole error case. The graph at the top left corner, with 8mm FWHM and 0mm maximum dipole location error, represents the best case scenario. It successfully captures the modeled connectivity dynamics: the red point shows connectivity from Frontal Mid Orbital (IC1) to Cuneus (IC3), the orange point shows connectivity from Frontal Inferior Triangularis (IC2) to the Angular Gyrus (IC4), the green points represent the spurious connections. When we increase FWHM, we see that FWHM of 16mm and 24mm confounds results by creating spurious connections that have high t-scores, to the point where the actual connections are weaker than spurious connections. The trend is similar for a 10mm maximum dipole location error, but not for 30mm, where a larger FWHM actually reduces t-scores of spurious connections and

helps locate the true connection from Frontal Mid Orbital (IC1) to Cuneus (IC3). The connection from Frontal Inferior Triangularis (IC2) to Angular Gyrus (IC4) is lost regardless of the FWHM, most likely because it operates at a higher frequency of 25Hz instead of 10Hz.

The maximum dipole location error is not a prior when processing any given dataset, but one telltale sign of a large error is that neighboring edges will display similar time-frequency connectivity measures. For example, in the graph for 8mm FWHM and 30mm maximum dipole location error, the bottom left corner shows two red points with similar t-scores. The points represent connectivity from Frontal Mid Orbital to Cuneus and to Occipital Superior, and their time-frequency plots were similar because they were caused by the same dipole. In this way, manual inspection at this stage can show whether a large maximum dipole location error exists and whether an acceptable FWHM was chosen. Therefore, limiting spurious connections is more important and we deduce that 8mm FWHM is a good starting point.

B. Actual Visual Hemifield Data

Bilateral versus Right did not produce any statistically significant results after GFWER correction, but Bilateral versus Left did. The pathway used during Right visual hemifield presentation may be the preferred pathway. Most of the edges that were significant (uncorrected $p \leq 0.01$) in Bilateral versus Left were also significant (uncorrected $p \leq 0.01$) in Left versus Right, so we chose to present the GFWER corrected ($p \leq 0.01,\ u = 10$) Left versus Right results. Five of eleven edges with

increased connectivity were from Left to Right, four were from Right to Left, and the remaining two were from Right to Right. In general, there was a heavy increase in interhemispheric interaction, which could be tied to increased efforts in accessing the preferred pathway. The right intrahemispheric interaction was consistent with the contralateral nature of visual processing. Remarkably, all eleven edges were pointed towards the sensorimotor areas of precentral and postcentral gyri. Unfortunately, the differences in connectivity of the sensorimotor areas was not associated with the response time differences, which were not significantly different between Left and Right.

The two most prominent connections were between Postcentral R and Precentral L. Fig 3.4 shows the time-frequency t-score plots in Left minus Right, Left, and Right, from Postcentral R to Precentral L. One prominent feature in the difference plot is the increase in activity in 18Hz for the whole epoch after the baseline; this 18Hz difference was also shown in some of the other edges. When examining the 18Hz activity in the Left and Right plots separately, we see that the Left condition has suppressed connectivity from 0 to 700ms and increased connectivity from 700ms to the end of the epoch, while Right has suppressed connectivity throughout the epoch after baseline. The average response time for this task was 580ms, and reprocessing the dataset with epochs time locked to response instead of stimulus could show interesting results. In both the Left and Right conditions, there is also a strong increase in low-frequency connectivity from 0 to 1s, which should be related to the P300; this activity was not significantly different and is not shown in the Left minus Right plot.

3.5 **Discussion**

We demonstrated an EEGLAB pipeline for estimating group-level brain connectivity. We compared dDTF08 and RPDC, and showed that the two methods are significantly different. dDTF08 was more appropriate for the simulated and actual data set presented, but may be outperformed by RPDC depending on the data and MVAR modeling parameters. We studied the interaction of Gaussian FWHM and maximum dipole location error, and propose that 8mm is a good starting point for FWHM. A large FWHM performed well in datasets with a high dipole locations error of 30mm, but generated many spurious connections in datasets with low dipole location errors. Regardless, dipole location errors are expected to decrease with improvements in EEG recording and in data processing algorithms, and datasets with high dipole location errors could be considered faulty. Furthermore, recent work shows asynchronous cortical generators producing measureable scalp signals [22], challenging the validity of dipole fitting and subsequently this connectivity analysis pipeline. For statistical analysis, bootstrap testing of time-frequency points avoids the common problem of circular analysis, or double dipping, in efforts to produce intelligible results by reducing dimensions of high-resolution EEG data. Finally, changing the many parameters in SIFT and Network Projection can lead to vastly different results. Given the nature of this data exploration tool, it may also be tempting to tune parameters until desired results are obtained; further research should be conducted to determine the optimal parameters.

3.6 Conclusion

In this chapter we discussed how graph theoretical brain connectivity analysis can be carried out in EEGLAB. The exploration of parameters was done not only to test the pipeline but also to provide users with an idea of how to select the proper parameters. We conclude that for this pipeline, dDTF08 is a more suitable brain connectivity estimator, and that a FWHM of 8mm should be sufficiently large. The demonstration with the actual visual hemifield data shows that this pipeline can be an effective tool in data exploration.

3.7 Acknowledgements

The work in Chapter 3 was carried out under the guidance of Makoto Miyakoshi, Gert Cauwenberghs, and Scott Makeig. The Source Information Flow Toolbox (SIFT) and Measure Projection Toolbox (MPT) were created by Tim Mullen and Nima Bigdely-Shamlo, respectively; the thesis author would like to thank Tim Mullen and Nima Bigdely-Shamlo for their advice, via e-mail and in-person at Qusp. The thesis author was the primary investigator and author of this work.

3.8 **Figures**

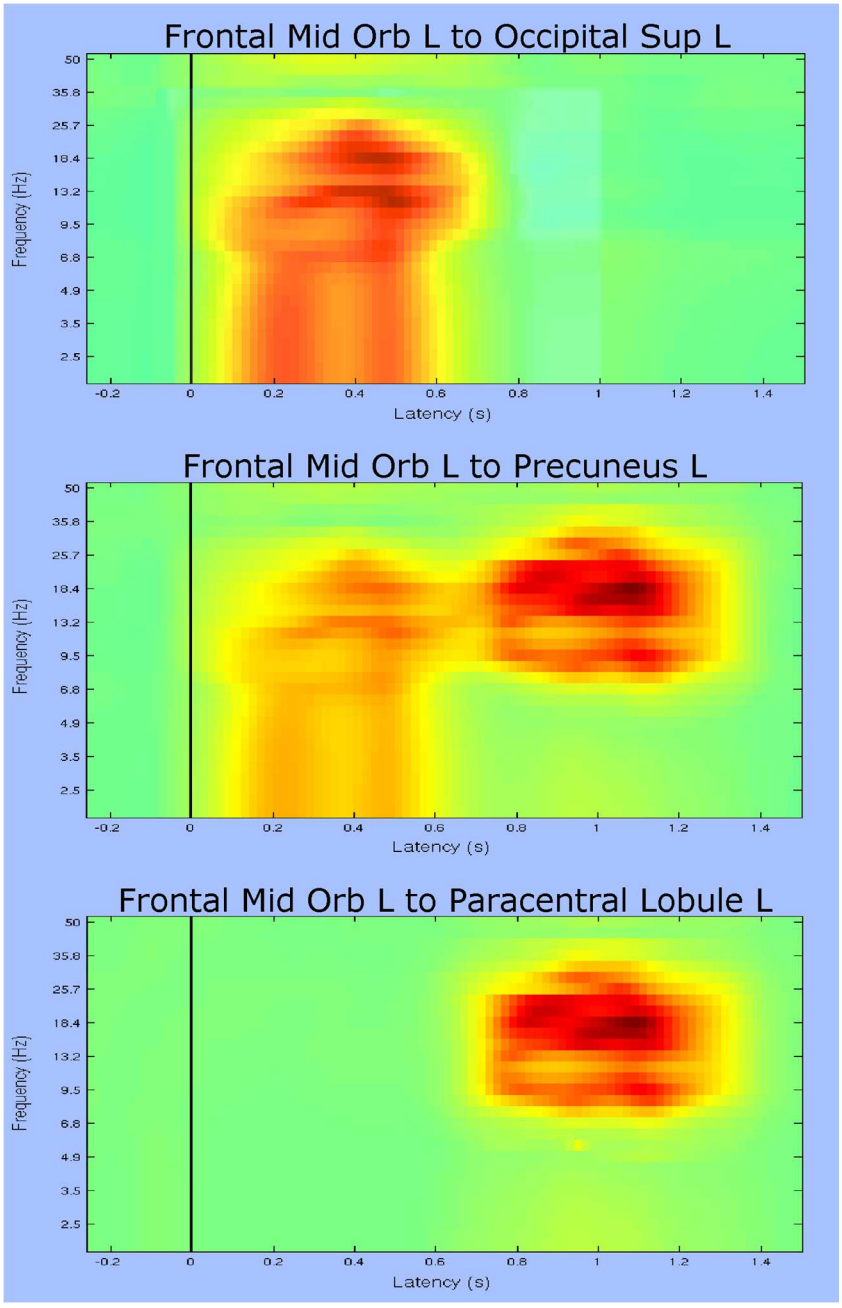

Figure 3.1. Time-frequency t-score plots showing negative effect of choosing an unsuitably large FWHM. Frontal Mid Orbital Left drives Occipital Superior Left (top) and Paracentral Lobule (bottom). Frontal Mid Orbital Left appears to drive Precuneus Left and the pair displays a spurious connection in the form of the union of connectivity measures from the neighboring regions (middle).

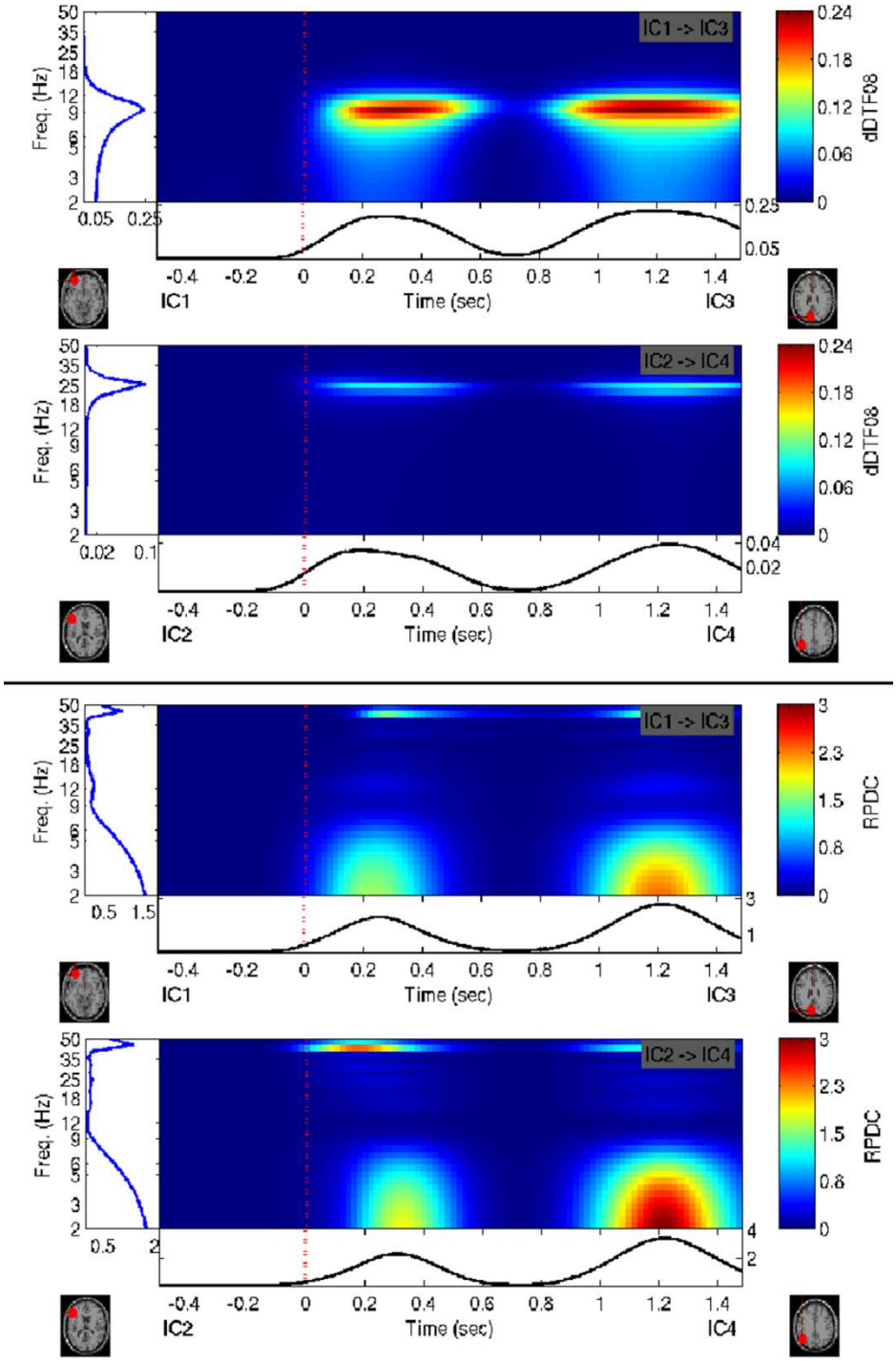

Figure 3.2. dDTF08 (top) versus RPDC (bottom) in a single simulated subject. dDTF08 is superior in capturing frequency spectrum.

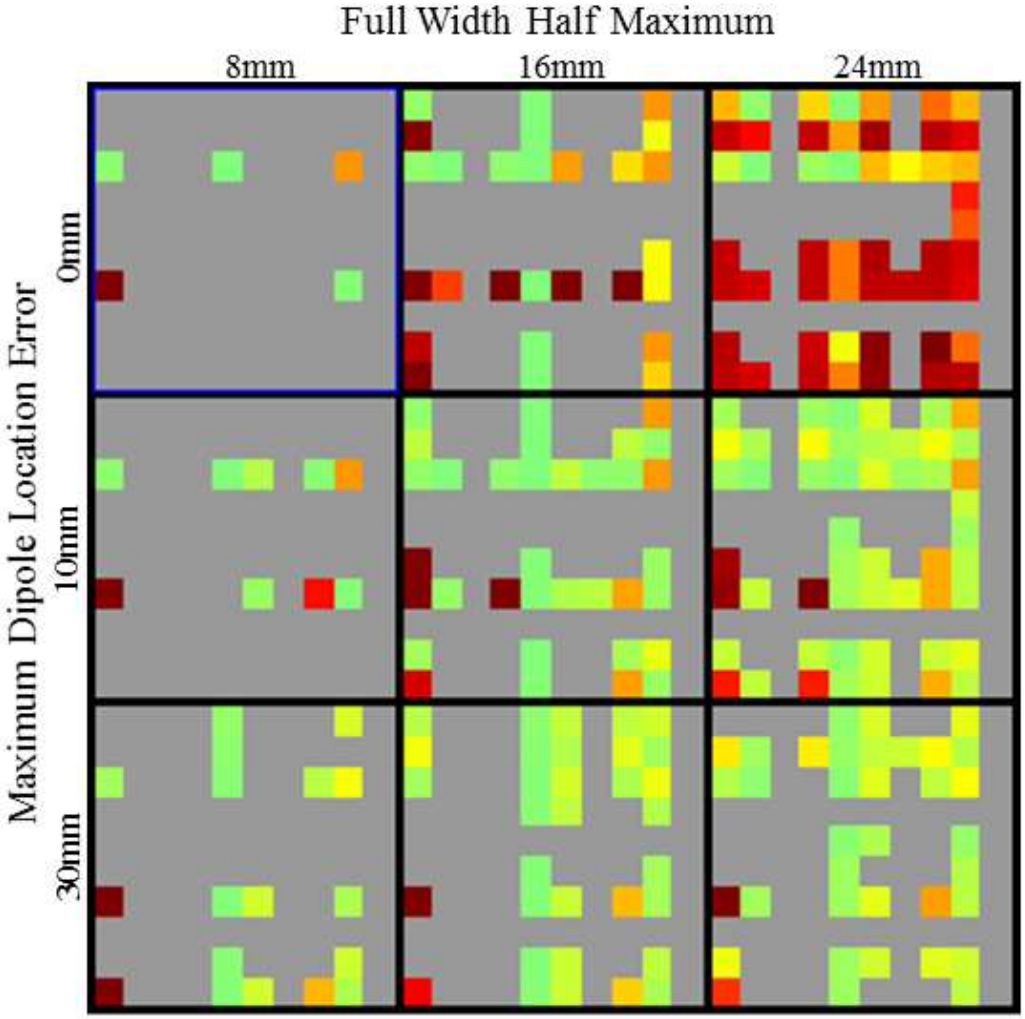

Figure 3.3. 3 x 3 case study of interaction between FWHM and Maximum Dipole Location Error. Top left corner (blue border) with 8mm FWHM and 0mm dipole location error is the best case scenario; the red and orange points represent simulated connections. Large FWHM generates spurious connections for small dipole location error.

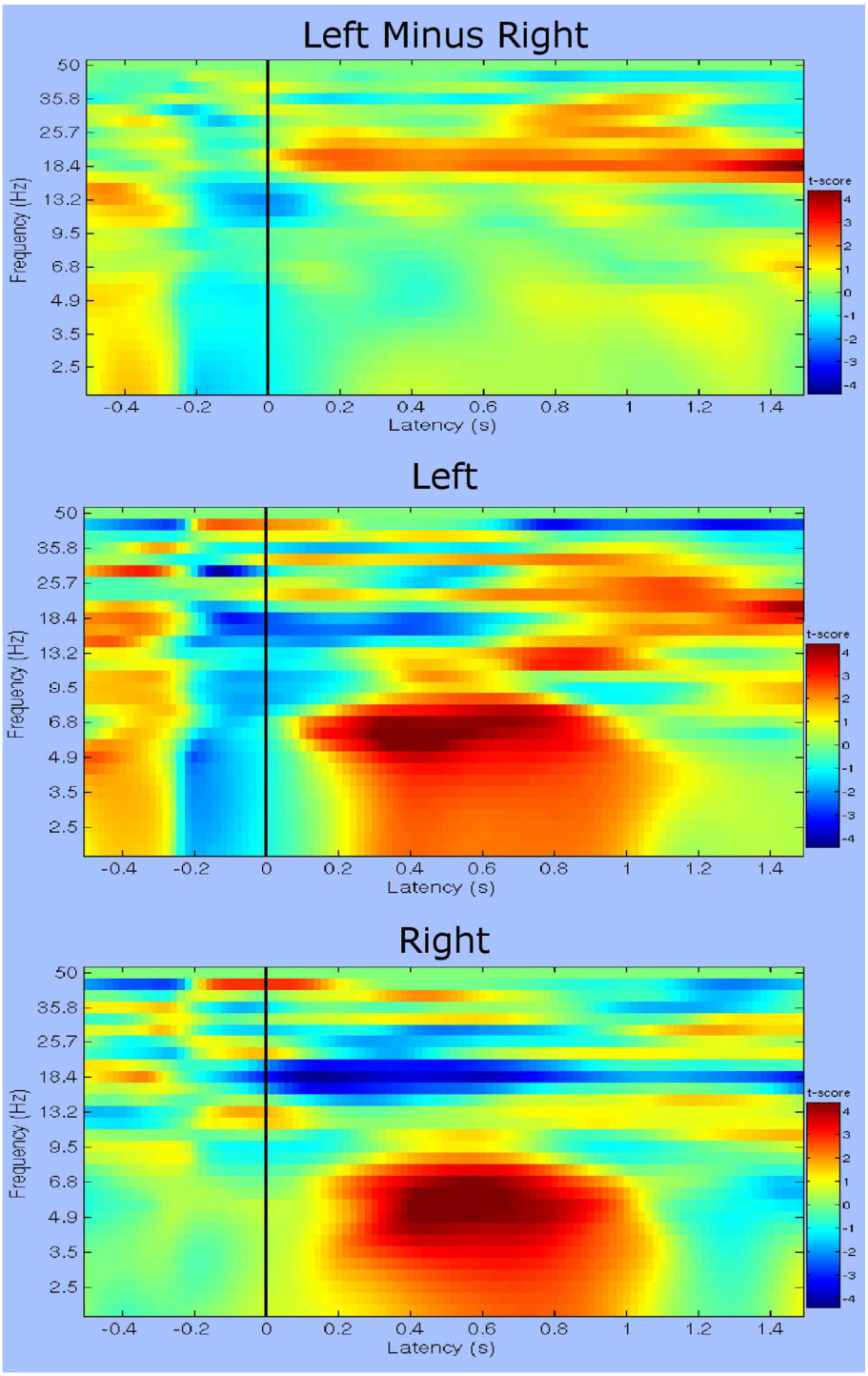

Figure 3.4. Time-frequency t-score plots for Postcentral R to Precentral L. Visual Field comparisons are Left Minus Right (top), Left (middle), and Right (bottom). Significant differences around 18Hz arises from increased connectivity in Left but suppressed connectivity in Right.

3.9 **Tables**

Table 3.1. Numbers and directionality of hemispheric interactions for the 3 x 3 case of full width at half maximum (FWHM) and maximum dipole location error.

		Hemispheric Interaction (number of edges)				
Max Error (mm)	**FWHM (mm)**	Left to Left	Left to Right	Right to Left	Right to Right	Total
0	8	80	0	0	0	80
	16	350	23	23	0	396
	24	733	63	63	0	859
10	8	189	9	9	0	207
	16	519	40	40	0	599
	24	752	79	79	3	913
30	8	333	27	27	0	387
	16	559	38	38	0	635
	24	668	61	61	4	794

REFERENCES

[1] S. Makeig, A. J. Bell, T. Jung, and T. J. Sejnowski, "Independent component analysis of electroencephalographic data.," in *Advances in Neural Information Processing Systems*, MIT Press, 1996, pp. 145–151.

[2] A. Delorme and S. Makeig, "EEGLAB: an open source toolbox for analysis of single-trial EEG dynamics including independent component analysis.," *J Neurosci Methods*, vol. 134, no. 1, pp. 9–21, Mar. 2004.

[3] A. Delorme, T. Mullen, C. Kothe, Z. Akalin Acar, N. Bigdely-Shamlo, A. Vankov, and S. Makeig, "EEGLAB, SIFT, NFT, BCILAB, and ERICA: new tools for advanced EEG processing.," *Comput Intell Neurosci*, vol. 2011, p. 130714, May 2011.

[4] K. J. Friston, "Modes or models: a critique on independent component analysis for fMRI.," *Trends Cogn Sci (Regul Ed)*, vol. 2, no. 10, pp. 373–375, Oct. 1998.

[5] J. Onton, M. Westerfield, J. Townsend, and S. Makeig, "Imaging human EEG dynamics using independent component analysis.," *Neurosci Biobehav Rev*, vol. 30, no. 6, pp. 808–822, Aug. 2006.

[6] A. Delorme, J. Palmer, J. Onton, R. Oostenveld, and S. Makeig, "Independent EEG sources are dipolar.," *PLoS ONE*, vol. 7, no. 2, p. e30135, Feb. 2012.

[7] A. J. Rissling, M. Miyakoshi, C. A. Sugar, D. L. Braff, S. Makeig, and G. A. Light, "Cortical substrates and functional correlates of auditory deviance processing deficits in schizophrenia.," *Neuroimage Clin,* vol. 6, pp. 424–437, Oct. 2014.

[8] A. Korzeniewska, C. M. Crainiceanu, R. Kuś, P. J. Franaszczuk, and N. E. Crone, "Dynamics of event-related causality in brain electrical activity.," *Hum Brain Mapp*, vol. 29, no. 10, pp. 1170–1192, Oct. 2008.

[9] B. Schelter, J. Timmer, and M. Eichler, "Assessing the strength of directed influences among neural signals using renormalized partial directed coherence.," *J Neurosci Methods*, vol. 179, no. 1, pp. 121–130, Apr. 2009.

[10] M. Kaminski and K. Blinowska, "A new method of the description of the information flow in the brain structures," *Biol Cybern*, vol. 65, no. 3, pp. 203–210, Jul. 1991.

[11] L. A. Baccalá and K. Sameshima, “Partial directed coherence: a new concept in neural structure determination.,” *Biol Cybern*, vol. 84, no. 6, pp. 463–474, Jun. 2001.

[12] H. H. Jasper, “The ten twenty electrode system of the international federation,” *Electroencephalogr Clin Neurophysiol*, 1958.

[13] R. Oostenveld and P. Praamstra, “The five percent electrode system for high-resolution EEG and ERP measurements.,” *Clin Neurophysiol*, vol. 112, no. 4, pp. 713–719, Apr. 2001.

[14] M. Kaminski and K. J. Blinowska, “Directed Transfer Function is not influenced by volume conduction-inexpedient pre-processing should be avoided.,” *Front Comput Neurosci*, vol. 8, p. 61, Jun. 2014.

[15] N. Bigdely-Shamlo, T. Mullen, K. Kreutz-Delgado, and S. Makeig, “Measure projection analysis: a probabilistic approach to EEG source comparison and multi-subject inference.,” *Neuroimage*, vol. 72, pp. 287–303, May 2013.

[16] X. H. Zhou, S. Gao, and S. L. Hui, “Methods for comparing the means of two independent log-normal samples.,” *Biometrics*, vol. 53, no. 3, pp. 1129–1135, Sep. 1997.

[17] D. M. Groppe, T. P. Urbach, and M. Kutas, “Mass univariate analysis of event-related brain potentials/fields I: a critical tutorial review.,” *Psychophysiology*, vol. 48, no. 12, pp. 1711–1725, Dec. 2011.

[18] Z. Akalin Acar and S. Makeig, “Effects of forward model errors on EEG source localization.,” *Brain Topogr*, vol. 26, no. 3, pp. 378–396, Jul. 2013.

[19] M. Miyakoshi, N. Kanayama, T. Iidaka, and H. Ohira, “EEG evidence of face-specific visual self-representation.,” *Neuroimage*, vol. 50, no. 4, pp. 1666–1675, May 2010.

[20] L. Barnett and A. K. Seth, “Behaviour of Granger causality under filtering: theoretical invariance and practical application.,” *J Neurosci Methods*, vol. 201, no. 2, pp. 404–419, Oct. 2011.

[21] N. Bigdely-Shamlo, T. Mullen, C. Kothe, K. M. Su, and K. A. Robbins, “The PREP pipeline: standardized preprocessing for large-scale EEG analysis.,” *Front Neuroinformatics*, vol. 9, p. 16, Jun. 2015.

[22] N. von Ellenrieder, J. Dan, B. Frauscher, and J. Gotman, “Sparse asynchronous cortical generators can produce measurable scalp EEG signals.,” *Neuroimage*, vol. 138, pp. 123–133, Sep. 2016.